Electronic Supplementary Information

Structure of Spontaneously Formed Solid-Electrolyte Interphase on Lithiated Graphite Determined Using Small-Angle Neutron Scattering

Robert L. Sacci,[a] *J. Leo Bañuelos,*[b†] *Gabriel M. Veith,*[a] *Ken C. Littrell,*[c] *Yongqiang. Q. Cheng,*[d] *Christoph. U. Wildgruber,*[d] *Lacy L. Jones,*[d] *Anibal J. Ramirez- Cuesta,*[d] *Gernot Rother,*[b] *Nancy J. Dudney*[a]

[a] Materials Science and Technology Division, Oak Ridge National Laboratory, Oak Ridge, TN 37831, USA.
[b] Chemical Sciences Division, Oak Ridge National Laboratory, Oak Ridge, TN 37831, USA. saccirl@ornl.gov
[c] Spallation Neutron Source, Oak Ridge National Laboratory, Oak Ridge, TN 37831, USA.
[d] High Flux Isotope Reactor, Oak Ridge National Laboratory, Oak Ridge, TN 37831, USA.

Corresponding Authors:
RLS, saccirl@ornl.gov; JLB, jose.banuelos@stfc.ac.uk

Materials Characterization. SEM images of the milled and unmilled graphites were acquired using a Hitachi S4800 and are shown in **Figure S1**. The qualitative distribution of particle sizes was developed using ImageJ64 by fitting circles to >50 particles from two images. This is also provided in **Figure S1**. Milling decreases the average particle size, broadens the size distribution, and changes the topology from spherical to disk-shaped. These are the cause of the increase in specific surface area measured by N_2 adsorption (Brunauer, Emmet, and Teller—BET), **Figure S2**. The N_2 and CO_2 BET measurements were performed with an Autosorb-1-C (Quantachrome Instruments) at 77 and 273 K, respectively. Presence of hysteresis at 0.45 in the isotherm confirms the presence mesoscale pores.

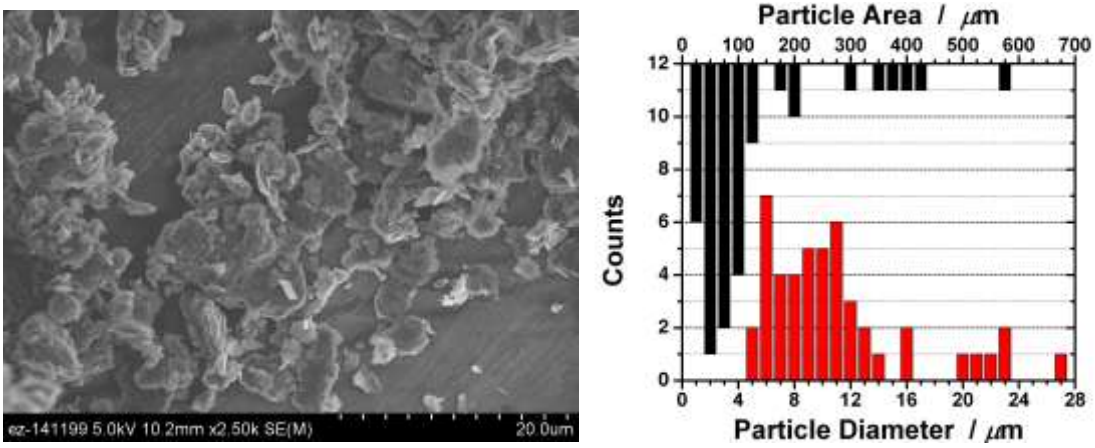

Figure S1: Representative SEM image of milled graphite (left) and the particle dispersion histogram taken from two different images. Particle areas were calculated on the particles used in the diameter measurement assuming a disk shape, *i.e.*, $A = \pi(2r^2 + hr)$.

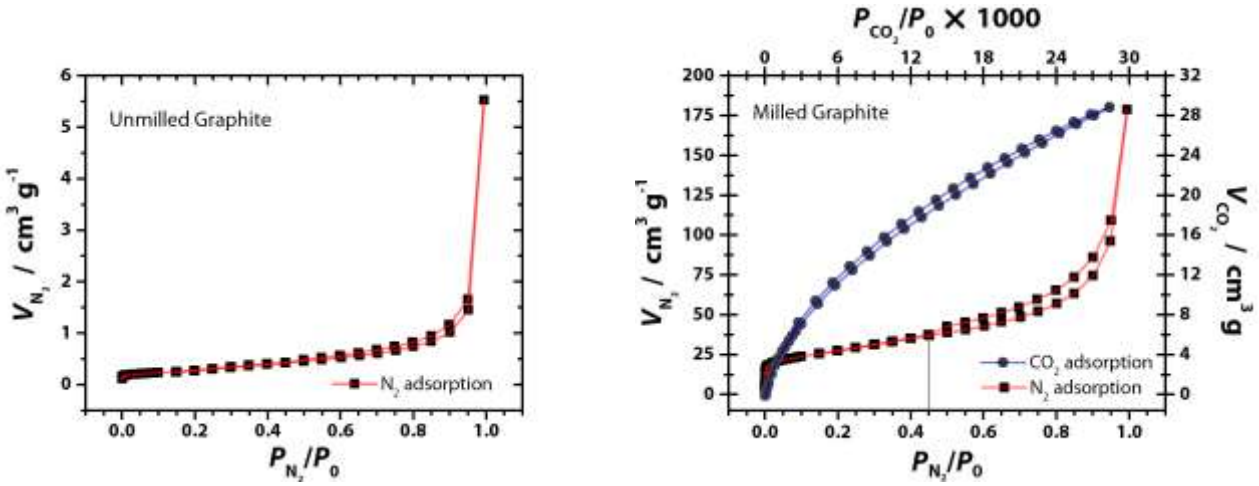

Figure S2. N_2 adsorption isotherm of unmilled (left) and milled (right) mesophase graphite with CO_2 adsorption isotherm. Vertical mark at 0.45 is used to highlight mesoporous behavior of the milled graphite.

X-ray diffraction (XRD) samples were prepared by decrimping the coin cells after the SANS measurement in an inert glovebox and sealing the powders between two 25 μm thick Kapton® films with TorSeal®. Measurements were conducted on an X'pert Pro diffractometer (PANalytic, Inc.) with Cu-K_α x-ray source operating at 45 kV and 40 mA. Scattering angles 10–100° were collected in 0.02° steps with a count time of 0.4 s per step. The spectra were indexed with powder diffraction files (HighScore Plus, ICDD and COD) 24-1079 for raw graphite, 34-1320 for LiC_6, 34-1326 for LiC_{12}, and 00-008-0768 for ethylene carbonate. Samples prepared in this manner were stable in ambient air for 8 hours. X-ray diffractograms of the starting carbons and the reacted are given in **Figure S3**. The (002) gallery spacing is a clear indicator of Li-C stoichiometry. The lithiated pristine material is 95% stoichiometrically pure. The products show more change in the LiC_{12} (002) region than that of LiC_6. That is, LiC_{12} reacted in greater amounts than LiC_6, thus agreeing with the greater SEI mass gain (Table 1).

SANS Experiments. The dried powders were loaded into a CR2032 stainless steel (s.s.) coin cell depicted in **Figure S4**. An aluminum washer defined the sampling volume (1 mm thick, 14 mm diameter). A s.s. spring was used to press the powders and had an inner diameter of 12 mm. To minimize scattering from the spring an 8 mm round aperture was used for the neutron beam. Standard data corrections include empty container scattering background, instrument dark current, detector efficiency, and the reduced data were placed on an absolute scale using internal calibration standards. The mass of each sample was used to obtain the sample packing density. Sample-specific subtraction of incoherent scattering was also made. In these types of samples, the presence of hydrogen in the non-deuterated, electrolyte-exposed samples caused a flat incoherent background, which was treated as a constant intensity across all *Q*-values and subtracted from the data presented in **Figures 3** and **5** of the main text. The background level was chosen with the aid of the PRINSAS software package[1], which found the best fit of a power law decay plus constant background at the high *Q* limit of the collected data.

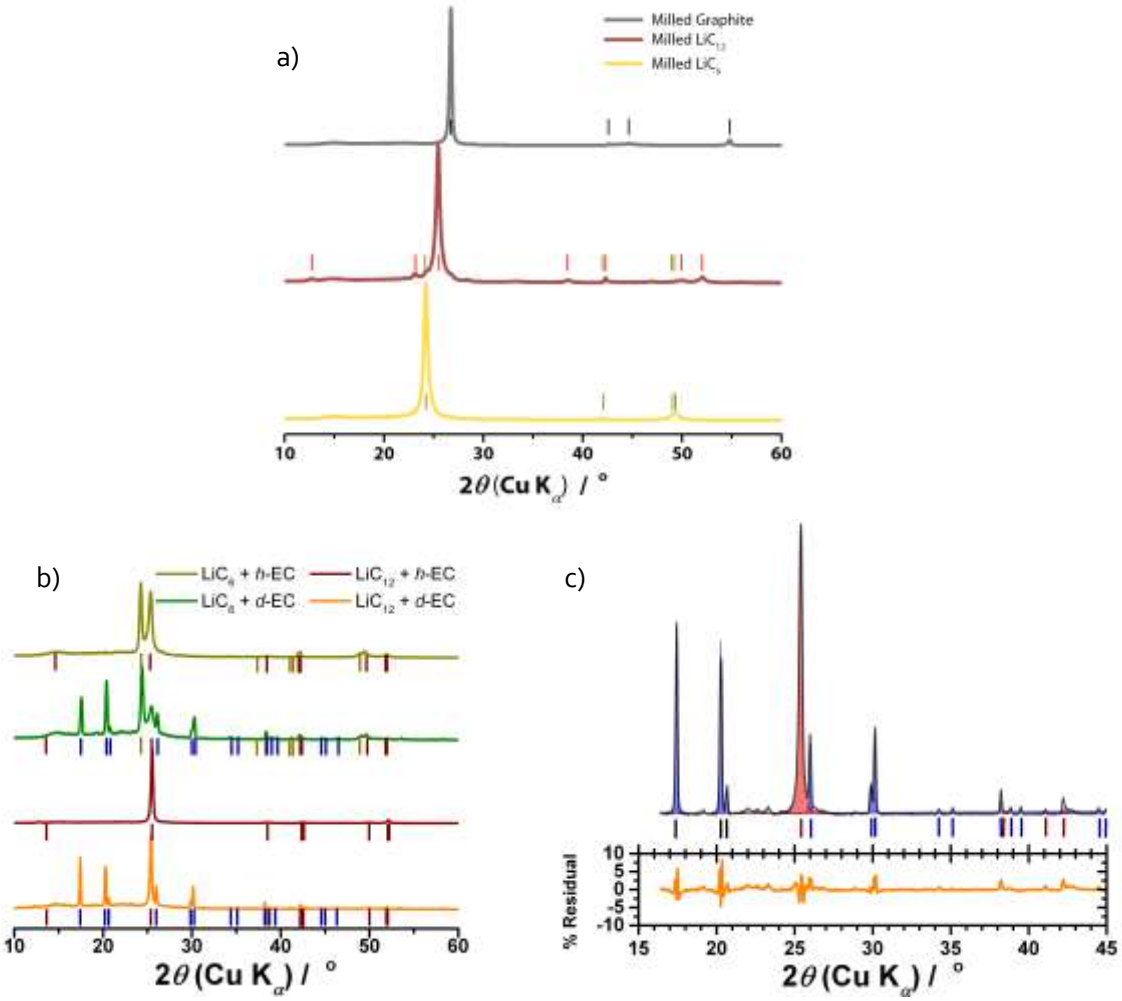

Figure S3. (**a**) XRD of the starting carbons. (**b**) Products from reacting LiC_6 or LiC_{12} with EC/DMC mixture used for SANS measurements. (**C**) Example of the Rieveldt refinement of the LiC_{12}+*d*-EC/DMC x-ray diffractograms in **Figure S3b**. Vertical lines mark the Bragg peak's phase: **gold**, LiC_6; **red**, LiC_{12}; **blue**, EC; **black**, graphite.

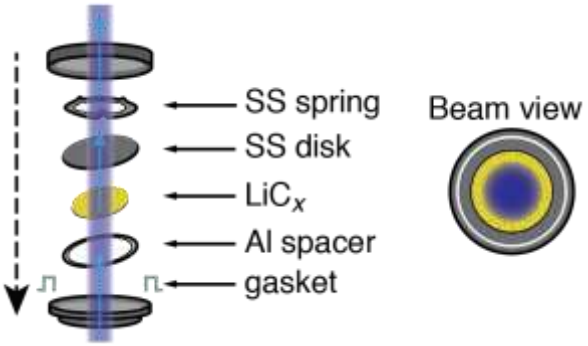

Figure S4. Schematic of the coin cell construction and sealing for the SANS experiment. Direction of crimping action is given by black arrow and blue arrows give the incident beam direction.

Comparison of pristine samples. The LiC_6, LiC_{12}, and non-lithiated graphite scattering curves are similar, as shown in **Figure S5.** This suggests that the surfaces in all of the pristine graphites are similar after the milling procedure. The slightly higher packing fraction and higher degree of scattering from 0.01 to 0.6 $Å^{-1}$ for the pure graphite samples indicates that there may be a different size distribution of the milled particles and a higher fraction of nano-sized inter-grain pore spaces in C_6. The scattering curve of graphite exposed to EC/DMC shows no reaction took place, the solvent is completely removed from intergrain spaces, and the original scattering curve of C_6 is recovered.

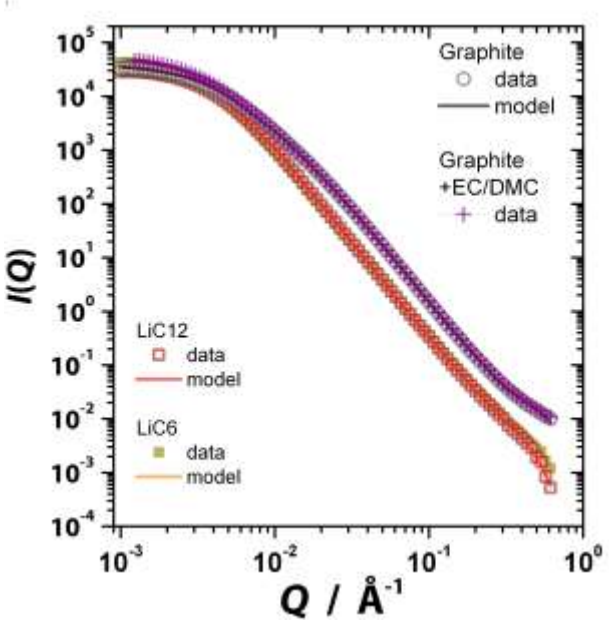

Figure S5. The SANS curves of the pristine carbons including the graphite–solvent control. The fitted curves are the product of modeling of a two-phase system (air and pristine carbon).

PRINSAS modeling. The fully reduced SANS data for the pristine carbon and lithiated carbons (C_6, LiC_6 and LiC_{12}), as well as LiC_6 and LiC_{12} exposed to the deuterated EC/DMC mixture were imported into the PRINSAS software package to determine the size dependence of the porosity in the pristine samples and the length scales at which porosity changes with exposure to electrolyte.

The scattering intensity per unit volume for a sample with a volume fraction φ of monodisperse spheres with radius r is given by:

$$I(Q) = (\rho_1 - \rho_2)^2 \varphi(1-\varphi) V_r F_{\text{sphere}}(Q\,r) \tag{1}$$

Here, ρ_1 and ρ_2 are the scattering length densities of the two phases (in our case, graphite and air/SEI), and V_r and $F_{\text{sphere}}(Q\,r)$ are the volume and form factor of a sphere of radius r, respectively. The program fits the scattering intensity by using a general distribution of spherical pores represented as a histogram (see **Figure 4** in main text):

$$I(Q) = \sum_i I\ \ Q_{0i} \frac{\int_{R_{\min,i}}^{R_{\max,i}} V_r^2 F_{\text{sphere}}(Q\,r) dr}{(R_{\max,i} - R_{\min,i})} \tag{2}$$

where the product is the contribution to $I(Q)$ of the i^{th} histogram cell with limits $R_{\min,i}$ and $R_{\max,i}$, *i.e.*,

$$I(Q) \cdot Q_{0i} = \frac{(\rho_1 - \rho_2)^2 \varphi}{\overline{V_r}} f(r_i)\left(R_{\max,i} - R_{\min,i}\right) \tag{3}$$

The porosity can be calculated from the equations above with the pore size distribution (PSD) being composed of the fitted $f(r_i)$. The specific surface area (SSA) is given by

$$\frac{S(r)}{V} = n_v \int_r^{R_{\max}} A_r f(r') dr' \tag{4}$$

where n_v is the average number of pores per unit volume, $A_r = 4\pi r^2$, and $S(r)$ is the total surface area of pores with radius larger than r. Further information may be found in the software reference.[1] The *Q*-range for the fits was 0.001 – 0.61 Å^{-1} and a bin size of 30 r-points per decade in *Q* was chosen for all fitted data. These values must be kept fixed between samples since they affect the normalization of the calculated SSA and PSD histograms.

The scattering contrast is defined as the NSLD difference between air and the carbon (Table 1 in the main text) and was used to obtain the nanoscale porosity of the unreacted carbons. Because the program only allows 2 phases in the calculation, the NSLD of the carbon was used to approximate the NSLD of both the carbon and the new electrolyte/SEI phase, and the approximate SSA and PSD of the available pore space in the samples reacted with deuterated electrolyte was calculated. Because the NSLD of the deuterated electrolyte is close to the value of the carbon, this approximation helps to identify the pore scales at which changes occur. The actual changes, however, are greater than the calculations because the NSLD of the electrolyte and predicted SEI is less than the carbon NSLD. We find an overall decrease in the porosity, with a larger relative decrease between 10–20 nm, as well as in pore sizes beyond 200 nm. The surface area decreases from the sub-nm to ca. 40 nm, in both LiC_6 and LiC_{12}. For r > 50 nm, LiC_6 shows little change and LiC_{12} shows an increase in the surface area. An increase in the surface area agrees with the observation that the surfaces become rougher (as observed from the surface fractal scattering) after exposure to the electrolyte.

Calculation of inter-grain pore components. The intensity at $Q = 0.014$ Å^{-1} is proportional to the square of the NSLD difference, $\Delta\rho^2$, between the LiC_x phase and the average composition inside the inter-grain pore, *i.e.*,

$$I(Q = 0.014) = A(\Delta\rho)^2/m_{C_x} \quad (5)$$

Here, $\Delta\rho = \rho_{\mathrm{LiC}_x} - \rho_{\mathrm{pore}}$, m_{C_x} is the carbon mass in the LiC_x substrate used for normalization, and A is a constant. ρ_{pore} can be extracted from the data if we treat ρ^*_{pore} to consist of three phases, namely a polymeric SEI phase $(1, \mathrm{polyEC})$, a solid EC phase $(2, \mathrm{solidEC})$ and empty space $(3, \mathrm{void})$:

$$\rho_{\mathrm{pore}} = c_1\rho^*_{\mathrm{polyEC}} + c_2\rho^*_{\mathrm{solidEC}} + c_3\rho^*_{\mathrm{void}} \quad (6)$$

Here, the c_i terms are the normalized concentrations such that

$$c_1 + c_2 + c_3 = 1 \quad (7)$$

Equations (6) and (7) can be combined to express c_2 as a linear function of c_1:

$$c_2 = \frac{1}{\rho^*_{\mathrm{solidEC}} - \rho^*_{\mathrm{void}}}\left[\left(\rho_{\mathrm{pore}} - \rho^*_{\mathrm{void}}\right) - c_1\left(\rho^*_{\mathrm{polyEC}} - \rho^*_{\mathrm{void}}\right)\right] \quad (8)$$

For $c_2 = 0$, as is the case for the non-deuterated EC/DMC-reacted samples, c_1 is expressed as

$$c_1 = \frac{\rho_{\mathrm{pore}} - \rho^*_{\mathrm{void}}}{\rho^*_{\mathrm{polyEC}} - \rho^*_{\mathrm{void}}} \quad (9)$$

and $c_3 = 1 - c_1$. The c_1 values from non-deuterated EC/DMC were used to constrain the possible compositions in the deuterated case that satisfy **Eq. (6)**. **Figure S6** shows a plot of the possible compositions in the deuterated case if no constraints on c_1 are applied. The values of c_1 for the non-deuterated case were used to find c_2 and c_3 for the deuterated case. This quantity is used to estimate the SEI thickness and the change in the inter-grain pore volume in the main text.

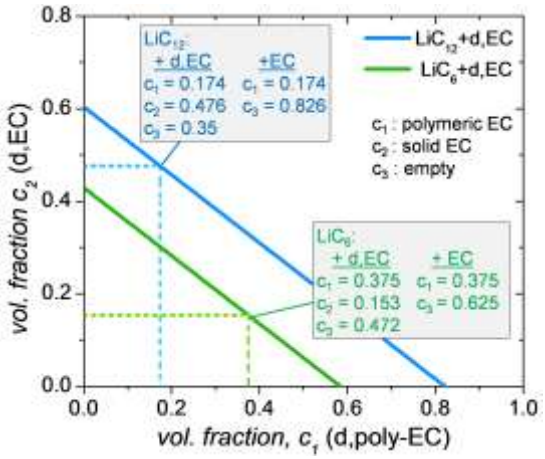

Figure S6. Calculated volume fractions of polymeric and solid EC within LiC_x.

1. Hinde, A. PRINSAS - a Windows-based computer program for the processing and interpretation of small-angle scattering data tailored to the analysis of sedimentary rocks. *J. Appl. Crystallogr.* **2004,** *37* (6), 1020-1024.